Characterization of Carbon Molecular Sieve Membranes Supported on Ceramic Tubes†

K. Briceño[1,*], J. Silvestre-Albero[2], A. Silvestre-Albero[2], J.I. Calvo[3], D. Montane[4], R. García-Valls[1], A. Hernández[3] and F. Rodríguez-Reinoso[2] *(1) Department d'Enginyeria Quimica, Universitat Rovira i Virgili, Av. Paisos Catalans, 26, E-43007, Tarragona, Spain. (2) Laboratorio de Materiales Avanzados, Departamento de Química Inorgánica, Universidad de Alicante, E-03080 Alicante, Spain. (3) Departamento de Física Aplicada, Facultad Ciencias, Universidad de Valladolid, E-47071 Valladolid, Spain. (4) Catalonia Institute for Energy Research (IREC), Bioenergy and Biofuels Division, Building N5, C/Marcel·lí Domingo 2, E-43007, Tarragona, Spain.*

(Received 5 October 2012; accepted 23 January 2013)

ABSTRACT: Carbon molecular sieve membranes have been analyzed in supported and unsupported configurations in this experimental study. The membranes were used to adsorb CO_2, N_2 and CH_4, and their adsorption data were analyzed to establish differences in rate and capacity of adsorption between the two types of samples (supported and unsupported). Experimental results show an important effect of the support, which can be considered as an additional parameter to tailor pore size on these carbon membranes. Immersion calorimetry values were measured by immersing the membranes into liquids of different molecular dimensions (dichloromethane, benzene, n-hexane, 2,2-dimethylbutane). Similarities were found between adsorption and calorimetric analysis. The pore volume of the samples analyzed ranged from 0.016 to 0.263 cm^3/g. The effect of the pyrolysis temperature, either 550 or 700 °C, under N_2 atmosphere was also analyzed. Quantification of the pore-size distribution of the support was done by liquid–liquid displacement porosimetry. The composite membrane was used for CO_2/CH_4 separation before and after pore plugging was done. The ideal selectivity factors value (4.47) was over the Knudsen theoretical factor (0.60) for membrane pyrolyzed at 600 °C, which indicates the potential application of these membranes for the separation of low-molecular weight gases.

INTRODUCTION

Previous studies have reported the application of carbon molecular sieve (CMS) materials in different gas separation applications (Ismail and David 2001). The turbostratic structure of CMS consists of an array of narrow constrictions at the entrance of micropores that are inter-connected through a system of galleries allowing separation of molecules based on their different shape and/or size. The amorphous character of these materials allows gases to diffuse through the constrictions at different adsorption rates (Foley 1995). Extended applications of CMS have been reported in industrial separation processes, e.g. N_2 separation from air (Chagger *et al*. 1995; Shirley and Lemcoff 1997). Their thermal stability and superior inertness when compared with other molecular sieves such as zeolites make them suitable for demanding applications, such as

* Author to whom correspondence should be addressed. E-mail: kellybm@gmail.com (K. Briceño).
†Published in the Festschrift of the journal dedicated to Professor K.S.W. Sing to celebrate his 65 years of research in the field of adsorption.

those involving temperature and elevated partial pressure of water. Furthermore, synthesis of molecular sieves based on carbon is simpler and cheaper than those based on other materials such as zeolites, whose methods are intricate and require additional post-treatments steps (Foley 1995). Beyond their use as adsorbents, CMS have been explored in the past for membrane applications (CMSM), building on the pioneering works of Rao (Rao and Sircar 1996) and Koresh (Koresh and Soffer 1987).

CMSM can be produced in different geometries—planar, hollow fibre and supported films—by pyrolysis of polymers at temperatures between 550 and 1000 °C (Saufi and Ismail 2004). The selection of membrane presentation depends on the final application of the membrane. Supported membranes are asymmetric structures that are preferred over the unsupported ones owing to their superior mechanical properties. However, even when using the same precursor, membrane properties can largely vary depending on the preparation procedure used. For example, in their attempts to reduce the number of coatings, Fuertes and Centeno (1999) reported differences between supported membranes obtained after three carbon-coating cycles and those obtained after deposition of three layers of the same precursor polyimide with a subsequent carbonization step. The latter sample exhibited higher permeation rates but lower selectivity compared with the former one. It is obvious that the way in which the carbon structure is formed depends on the coating procedure, which is responsible for differences in the properties of the carbon layer. Singh-Goshal and Koros (Singh-Ghosal and Koros 2000) outlined that it is easier to compute entropic selectivity on dense symmetric films than on asymmetric membranes.

Identification of the carbon structure becomes more complex if variables that are often considered to affect the carbon structure of flat membranes have to be considered on asymmetric configurations. Vu *et al*. (2002) confirmed an unexpected decrease in the CO_2 permeance values for CMS fibres (asymmetric membranes) after pyrolysis. On the contrary, permeance increased in planar films made from the same polymer (unsupported) following the same pyrolysis conditions. Apparently, when the polymer precursor is pyrolyzed in an asymmetric structure, as is the case of hollow fibre or supported samples, the carbonaceous structure obtained after pyrolysis becomes different from those samples obtained in a planar shape and dense film. It could be hypothesized that the presence of the support could determine differences in carbon structure because of the differences in the properties of the carbon layer.

The reasons explaining this difference have been scarcely explored in the past because it is not easy to characterize the changes in pore structure of these materials. In fact, characterization of unsupported carbon films has been used in the past to explain the morphological changes of its supported counterparts (Fuertes and Centeno 1999; Sedigh *et al*. 2000). However, little evidence has been shown in the past to understand the extent of this extrapolation. In addition, excluding permeance analysis, there are few studies that match the characterization of the overall supported membrane and its isolated carbon supported layer.

The aim of this work is to identify structural differences and similarities between carbon samples obtained in supported tubes and those obtained in unsupported planar configuration. The effect of coating layer on modification of a ceramic support has been explored using liquid–liquid displacement porosimetry (LLDP), a characterization technique that can distinguish active pores, thus contributing to actual flux, from those that do not actually inter-connect both sides of the membrane. Although it is not an objective of this work to propose a mechanism of carbon formation, a correlation has been found between the characteristics of the composite membrane and the structure of the carbon layer obtained.

MATERIALS AND METHODS

Preparation of Asymmetric Carbon Membranes

The carbon precursor used in our experiments was a polymeric material called Matrimid (3,3′,4,4′-benzophenonetetracarboxylic dianhydride and diaminophenylindane; Huntsman Advanced Materials). The carbon precursor was dissolved in 99.5% 1-methyl-2-pirrolydone (Sigma-Aldrich) at 13% w/w concentration. The solution was coated once (using a pipette) on a TiO_2/ZrO_2 macroporous ceramic support (Tami 1 kD membrane of 10 cm length × 4 cm outer radii) under rotation. After controlled drying, polymer-coated supports were placed in an oven at 300 °C under air atmosphere. This coated support was designated as supported (S) polymer (P), S_P300. In order to obtain carbon (C)-supported samples, two more membranes were prepared by with a higher pyrolysis temperature (550 and 700 °C), designated as S_C550 and S_C700, respectively. The pyrolysis treatment was performed under an N_2 atmosphere at a total flow rate of 500 ml/minute using a heating rate of 1 °C/minute. To compare supported with unsupported samples, a solution of the same concentration of polymer was casted on a glass support. After applying the same drying process previously described for supported samples, the film was extracted and placed on a ceramic vessel to allow it to be pyrolyzed under the same experimental conditions as described earlier. The unsupported (NS) samples were designed as NS_C550 and NS_C700 to identify those pyrolyzed at 550 and 700 °C. The morphology of the synthesized samples (supported and unsupported) was analyzed by scanning electron microscopy (SEM) after sputtering with Au. For the characterization of the supported samples, the carbon membrane was concentrated by scratching the carbon layer from the ceramic support using a small knife followed by an additional treatment with hydrofluoric acid (Sigma-Aldrich 48 wt % in water) for 2 minutes at 60 °C in order to eliminate the remaining TiO_2/ZrO_2 particles completely (Shimada *et al*. 1998).

Sorption Measurements

All materials were characterized by adsorption of probe molecules of different dimensions (CO_2, CH_4 and N_2) at different temperatures (–196 °C for N_2 and 0 °C for CO_2 and CH_4). The respective kinetic dimension diameters of the gases used were 0.36 nm (N_2), 0.33 nm (CO_2) and 0.39 nm (CH_4). Before performing the adsorption experiments, samples were outgassed under vacuum at 250 °C for 4 hours (Fuertes 2000; Briceño *et al*. 2010). Time of equilibrium for the different adsorption experiments was defined at 120 seconds.

Immersion Calorimetry

Immersion calorimetry measurements were performed at 30 °C by immersing the samples into liquids of different molecular dimensions: [dichloromethane (DCM; Aldrich, 99.5%), benzene (Aldrich, 99.8%), n-hexane (Aldrich, ≥ 97%), 2-methylpentane (Fluka, ≥ 99.5%) and 2,2-dimethylbutane (Aldrich, 99%)] using a Setaram C80D calorimeter. Before performing each experiment, the sample was degassed under vacuum (10^{-3} Pa) at 250 °C for 4 hours in a glass bulb; the bulb was later sealed and placed inside the calorimetric unit that contained the immersion liquid. Once the thermal equilibrium was reached, the bulb was broken allowing the liquid to penetrate into the bulb and be in contact with the sample. The heat released was followed as a function of time (Silvestre-Albero *et al*. 2001).

LLDP

LLDP was performed as described elsewhere (Calvo *et al*. 2008; Peinador *et al*. 2010). Before being placed in the porosimetric cell, the supported polymer and carbon membranes were cut into pieces of 4 cm length that were sealed at both ends with a ceramic aspect enamel painting (Titanlux) 24 hours before the porosimetric test. The liquid mixture used to perform the LLDP measurements was a mixture of isobutanol/methanol/water (15:7:25 w/w). The separated aqueous-rich phase was drained off and used as the wetting liquid and the alcohol-rich phase was used as the displacing liquid. In order to achieve complete wetting of membrane samples, carbon-supported membranes were immersed into the LLDP wetting phase for half-an-hour under vacuum (150 mmHg) at room temperature. Pore size was determined after pore depleting (flux-pressure plots). The mean pore size and the pore flow distribution of active pores were obtained from contributions to total flux, using an algorithm described in previous works (Peinador *et al*. 2010). From this flow distribution, and applying the Hagen–Poiseuille model for convective flow through capillary pores, flow distributions were converted into pore number distributions, which can be used to estimate the cut-off values of the analyzed membranes, as described elsewhere (Calvo *et al*. 2011).

Permeance Measurements

Pure gases (CO_2 and CH_4) were fed into the module at a transmembrane pressure difference of 1 bar. Argon gas was used as a carrier and the gas composition at the exit was followed using a mass spectrometer. The permeance of supported carbon membranes was determined according to calibration curves previously established. A tubular stainless steel module, 63 mm length, o.d. = 30 mm, i.d. = 12.2 mm, containing the tubular composite membrane was fitted with Viton O-rings that allowed the membrane housing in the module without leakage. In order to plug pinholes or defects in the composite membrane, supported carbon membranes were dip coated on a 12% wt. polydimethylsiloxane (PDMS; Sylgard@ 10:1 precursor:catalyst) solution in n-hexane (Aldrich).

RESULTS AND DISCUSSION

The morphology of carbon membranes was analyzed by SEM. Figure 1 shows micrographs of unsupported samples obtained after pyrolysis of the polymer at 550 and 700 °C, respectively. As it can be observed, the unsupported membranes are highly dense. The average thickness of the unsupported membranes is approximately 200 mm. Interestingly, the situation drastically changes for the supported membranes. As it can be observed in Figure 2, these membranes exhibit a lower density owing to the presence of big holes and cavities not observed in the unsupported configuration. Apparently, the supported carbon film maintains similarities with the mesoporous structure of the inorganic support, as it seems to copy the surface structure.

Sorption Measurements

Sorption measurements were carried out to study the effect of the porous support on the textural properties of the carbon layer, as well as the effect of the pyrolysis temperature. Adsorption isotherms allow for drawing conclusions about the porous structure of the material. The quantity of gas adsorbed by the adsorbent varies depending on the material structure and test conditions (pressure and temperature). The adsorption isotherms in microporous and mesoporous materials

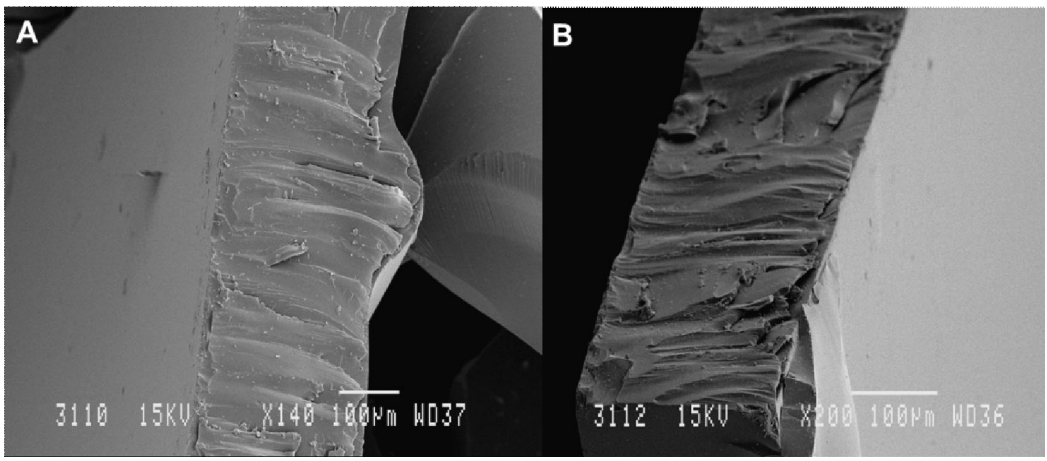

Figure 1. Unsupported carbon obtained at (A) 550 °C and (B) 700 °C.

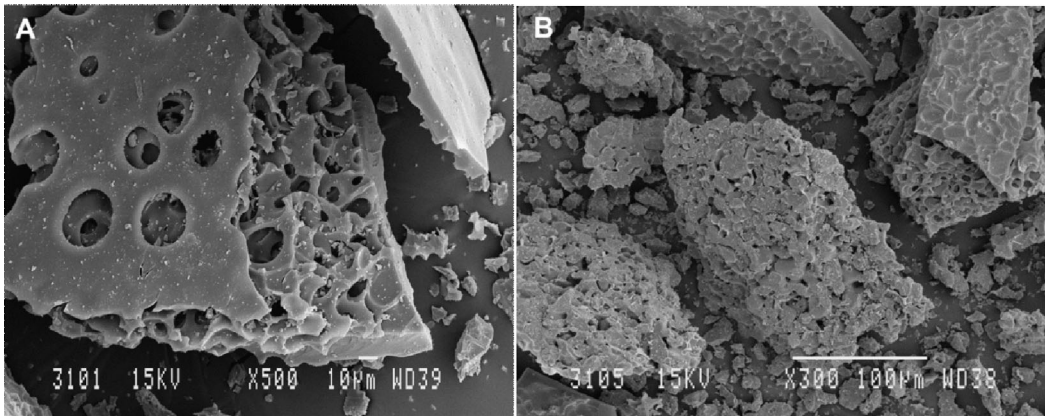

Figure 2. Supported carbon obtained at (A) 550 °C and (B) 700 °C.

are well defined and they can be classified according to the IUPAC recommendation as type I, for purely microporous solids, and a combination of types I and IV for materials that exhibit both micro- and mesoporosity (Sing *et al*. 1985). Eventually, deviations from these trends can be observed when the sample is not homogeneous or there are kinetic restrictions, i.e. cavities of molecular dimensions were probe molecules having problems of accessibility. This would imply that the desorption branch does not follow the path of the adsorption branch. In this sense, the use of different gases such as N_2, CO_2 and CH_4 with differences in kinetic diameters will allow for extracting differences between materials porosity.

N_2 adsorption was null in the synthesized materials, both supported and unsupported, thus anticipating the presence of narrow constrictions on these membranes inaccessible to nitrogen at cryogenic temperatures (–196 °C). A similar observation was reported by Favvas *et al*. (Favvas *et al*. 2007). The dimensions of the pores and constrictions of these CMSs must be comparable to the kinetic diameter of the N_2 molecule and, consequently, the diffusion of this gas at cryogenic temperatures (–196 °C) is low producing no adsorption in the conventional time of the measurement (Rodríguez-Reinoso *et al*. 1982; Rios *et al*. 2007).

Figures 3 and 4 show the adsorption isotherms for CO_2 and CH_4 on supported and unsupported samples at 0 °C, respectively. The amount of gas adsorbed, expressed in mmol of gas adsorbed per gram of adsorbent, is plotted as function of equilibrium pressure. As expected, the adsorption capacity is larger in all samples for a smaller molecule such as CO_2 compared with CH_4, with a larger kinetic diameter (0.39 nm versus 0.33 nm). The adsorption of these two gases at 0 °C confirms that N_2 adsorption at –196 °C was kinetically restricted because of the low temperature of the adsorption measurement, as the nitrogen molecule is smaller than methane. Furthermore, it is interesting to highlight that the isotherms for non-supported samples (Figure 3) are not reversible, i.e. they exhibit hysteresis. The shift between the adsorption and the desorption branches in the sorption isotherm clearly reflects the difficulty in these samples to reach equilibrium, as expected for molecular sieves, even at the high temperature of the adsorption measurement (0 °C).

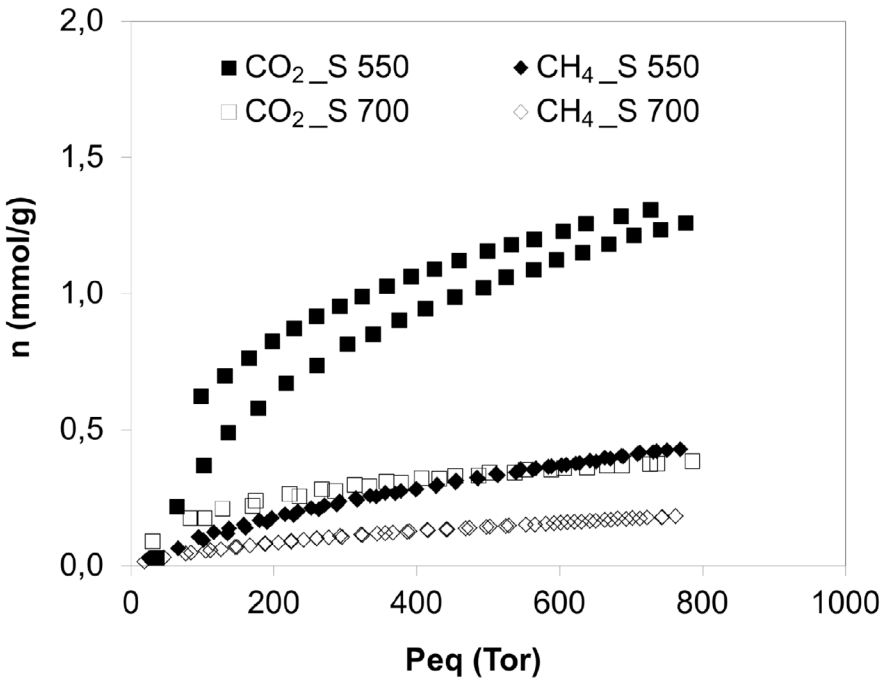

Figure 3. CH_4 and CO_2 adsorption–desorption isotherms at 0 °C for the different carbon non-supported membranes obtained at 550 and 700 °C pyrolysis temperatures.

When comparing supported and unsupported samples, the adsorption capacity is always lower in the supported configuration when using the same pyrolysis temperature, i.e. the presence of the support becomes detrimental for the final textural properties of the membrane. Finally, an increase in the pyrolysis temperature from 500 to 700 °C gives rise to a decrease in the total adsorption capacity for CO_2 and CH_4 for the supported samples (Figure 3), whereas the opposite trend is observed for the unsupported configuration (Figure 4). These results clearly suggest that (1) the porous structure of the synthesized membranes highly depends on the presence of the underlying support, i.e. the presence of the support results in a shrinkage of the porosity and (2) the stability of these membranes towards an increase in the pyrolysis temperature is also highly sensible to the final structural conformation.

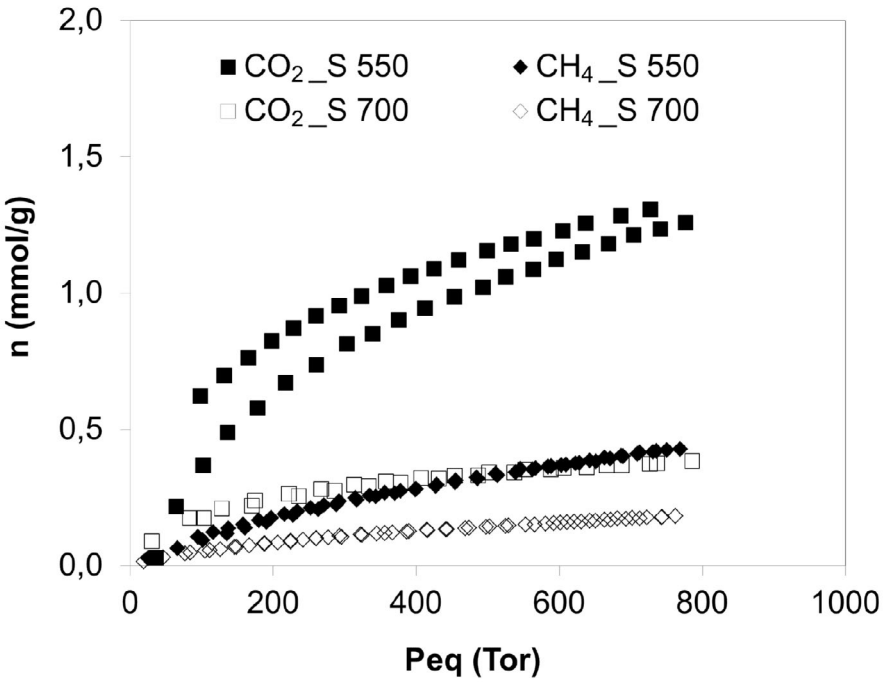

Figure 4. CH_4 and CO_2 adsorption–desorption isotherms at 0 °C for the different carbon-supported membranes obtained at 550 and 700 °C pyrolysis temperature.

The different effect of the pyrolysis temperature on the textural properties of supported and unsupported samples can be explained based on their morphological differences. An SEM analysis described earlier showed that the supported samples somehow copied the structure of the underlying support in contrast to the unsupported samples. It could be contradictory to think that the more porous sample (supported) has less adsorption capacity than the dense sample (non-supported). However, we have to consider that the type of porosity copied by the supported sample is in the mesoporous range whereas the adsorption–desorption analysis for CO_2 and CH_4 takes place mainly in the microporous structure. Most probably, the supported sample has a different asymmetric structure than non-supported samples. Moreover, the pyrolysis temperature and the support also affect the narrow microporosity of the membrane, i.e. differences not only in the morphology but also in the pore-size distribution for each type of samples. In this sense, Briceño and co-workers (Briceño *et al*. 2012a) showed the limiting effect of the support, using atomic force microscopy and wide angle X-ray diffraction, in the formation of graphite-like domains of the nanoporous carbon.

In unsupported samples the adsorption capacity increases with pyrolysis temperature, implying an increase in the pore size and volume. For the same type of polyimide, Steel and co-workers (Steel and Koros 2003) reported an increase in the volume fraction of pores in the order of $0.4 < x < 0.68$ nm when the final pyrolysis temperature was increased from 550 to 800 °C. In fact, they reported an increase of the integral pore volume from 0.08 cm^3/g at 550 °C to 0.10 cm^3/g at 800 °C and outlined the differences in pore-size distribution for both types of temperatures. They also remarked pore volume values as the determinant factor on equilibrium sorption. In addition, in the analysis done with unsupported Kapton, Suda and Haraya (1997) reported micropore volumes

using sorption isotherms of probe molecules with different kinetic diameters. They observed a decrease in pore volume and pore size with an increase in the pyrolysis temperature. The pore volume changed from 0.22 to 0.15 cm^3/g when temperature changed from 600 to 1000 °C. The effect of pyrolysis temperature can differ even when considering the same type of polymer. For example, Lua and Su (2006) reported an increase in CO_2 uptake with pyrolysis temperature for Kapton polyimide membranes obtained between 550 and 1000 °C. In fact, they remarked that up to 600 °C a large portion of micropores and mesopores are created but between 600 and 800 °C large pores shrink in parallel with the formation of new micropores due to H_2 evolution during this stage of pyrolysis.

In the case of supported samples it is more common to find a maximum pyrolysis temperature for optimum permeance. Above that pyrolysis temperature, permeance and adsorption capacity decrease again implying a decrease in pore volume due to pore shrinkage. In this sense, Hayashi *et al*. (1995) reported an increase in the permeance of CO_2 for a supported film of polyimide 3,3′,4,4′-biphenyltetracarboxylic dianhidride–4,4′-oxydianiline membrane after pyrolysis between 500 and 900 °C. Permeance reached a maximum at 650–700 °C, and the maximum micropore volume was near 800 °C, with decreasing values above that temperature.

Similarly, Centeno *et al*. (2004) reported the development of pores near 500 °C and their subsequent enlargement between 700 and 800 °C when a phenolic resin was supported on a ceramic tubular porous support of 20-nm pore size diameter. Afterwards, pores suffered shrinkage and complete collapse near 1000 °C. Those results support the existence of an optimal temperature to maximize pore volume development, after which shrinkage or enlargements probably occurs.

Differences on both types of membranes (supported and unsupported samples) can be observed in this work in close agreement with the literature. Moreover, these differences are more difficult to establish because they depend on the type of precursor used. Suda and Haraya (1997) already outlined that polyimide membranes could present a higher presence of amorphous regions or larger pores that could bring different structure and eventually different properties. Most probably, unsupported samples must exhibit larger amorphous regions than supported samples. This effect is more important when pyrolysis temperature is also present. In both types of samples, the presence of hysteresis in the sorption isotherms reflects the presence of a heterogeneous porous structure with narrow constrictions, i.e. kinetic restrictions are present. A delay on the desorption branch implies problems of equilibrium on the adsorption branch due to the presence of small pores/constrictions where the gas molecule has accessibility problems, and the desorption branch remaining above the adsorption branch down to very low pressures (Silvestre-Albero *et al*. 2012). The reason that explains the differences between the two types of samples could be that for each system different pore-size distributions determine the final adsorption–desorption capacities. Steel and co-workers (Steel and Koros 2005) mentioned that there could be a tail of ultramicroporous pores in the size distribution that would determine the quantity of pores available for smallest molecules while rejecting those with higher dimensions.

Immersion Calorimetry

In order to achieve a detailed pore size characterization, immersion calorimetry was performed by immersing the samples into liquids of different molecular dimensions such as DCM (0.33 nm), benzene (0.37 nm), n-hexane (0.43 nm) and 2, 2-dimethylbutane (0.56 nm) (Silvestre-Albero *et al*. 2001). As described in the previous section, molecular accessibility seems to be limited by the pore mouth on these carbon materials; an idea of the pore size, shape and pore volume can be extracted after calorimetric screening with several molecules of different molecular dimensions.

Figure 5 shows that both unsupported and supported carbon samples exhibit micropores around or below 0.33 nm, which is reflected in a large heat of immersion into a small molecule such as DCM. Increasing probe molecular size gives rise to a drastic decrease in the heat of immersion, i.e. a limited accessibility. In this sense, non-supported samples do not have microporosity above 0.43 nm due to the low or null heat of immersion of these samples when using n-hexane as a probe molecule. On the contrary, supported samples present some heat of immersion even for n-hexane, meaning that the pore size of supported membranes is slightly wider than for the unsupported ones, i.e. the supported membranes exhibit a wider pore-size distribution. For all samples evaluated, the limiting pore size value is determined to be below 0.56 nm due to the small heat of immersion when using DCM, i.e. DCM accessibility is mainly nil.

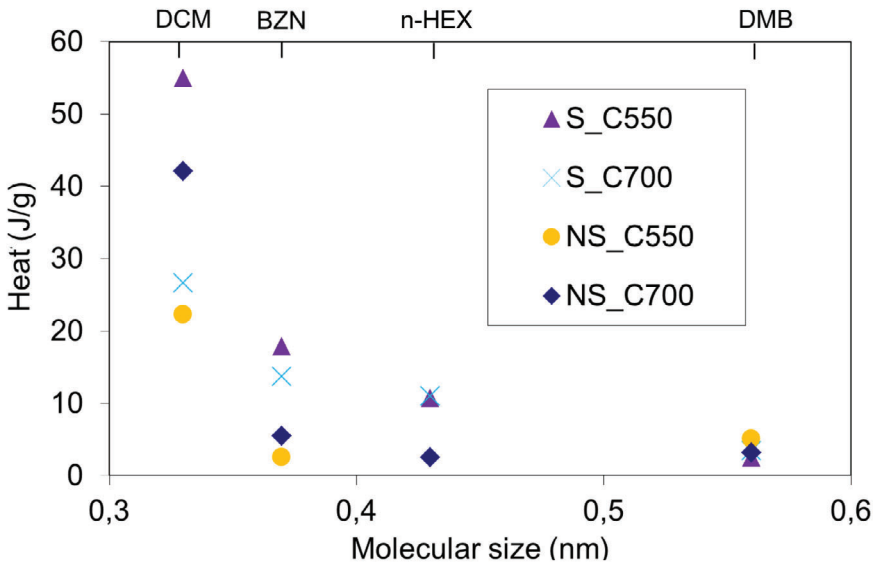

Figure 5. Enthalpy of immersion (J/g) for the different supported and unsupported samples into liquids of different molecular dimensions [dichloromethane (DCM), benzene (BZN), n-hexane (n-HEX), 2,2-dimethylbutane (DMB)].

Furthermore, it is interesting to highlight the nice agreement between the adsorption results when using small molecules such as CO_2, with a kinetic diameter of 0.33 nm, and immersion calorimetry measurements using a molecule with similar dimensions as DCM (0.33 nm). Taking into account that immersion calorimetric measurements are free of kinetic restrictions, the similarity between both measurements concerning the effect of the final conformation (supported or unsupported) and the effect of the pyrolysis temperature in the evolution of the porosity, validates the adsorption results described earlier.

For supported samples, an increase in the pyrolysis temperature gives rise to a decrease in the heat of interaction with DCM, which is in close agreement with CO_2 adsorption results. By contrast, when samples are unsupported, an increase in the pyrolysis temperature produces an increase on the heat of interaction in the same way as the adsorption capacity does.

It is important to outline that carbon materials usually contain slit-shaped micropores. In this sense, immersing the samples into benzene (immersion calorimetry) can be used as an extra tool to discern the shape of the microporosity (either cylindrical or slit shaped). According to Figure

5, all samples exhibit a gradual decrease in the heat of immersion from DCM (0.33 nm) to 2,2-dimethylbutane (0.56 nm). The larger heat of immersion for benzene in all samples compared with n-hexane clearly suggests that benzene is accessing the inner porous structure is a planar configuration (benzene, a disc-shaped molecule has a thickness of 0.37 nm and a diameter of 0.57 nm), and consequently, it is a confirmation of the slit-shaped micropores in these samples (at least the supported membranes). For the unsupported samples, this behaviour was not identified distinctly, but we would expect a similar shape.

From the heat of immersion into DCM and after the appropriate calibration using a standard non-porous carbon, the accessible surface area for a given liquid can be calculated. Table 1 shows the values of the accessible surface area for DCM in all carbon samples studied. The surface area accessible to DCM ranges from 200 to 500 m^2/g. Table 1 also reports micropore pore volume obtained after applying the Dubinin–Radushkevich equation to the CO_2 adsorption data. As described previously in the sorption analysis, the influence of pyrolysis temperature is not the same in both types of supported and unsupported samples. Narrow micropore volume decreases for supported samples after increasing pyrolysis temperature, whereas the opposite behaviour is observed for unsupported samples, which is in close agreement with calorimetric analysis.

TABLE 1. Surface Area Estimated by Immersion Calorimetry into Dichloromethane Together with the Narrow Micropore Volume Estimated from the CO_2 Adsorption Data at 0 °C

Sample	Area (m^2/g)	Narrow micropore volume (cm^3/g)
S_C550	488	0.017
S_C700	236	0.016
NS_C550	197	0.102
NS_C700	374	0.263

Modification and Characterization of the Macroporous Structure

In the last section, the microporous character of the membranes was investigated by analyzing the microporosity, which is the main parameter related to the selectivity of CMSMs. However, the support can affect the optimal performance of composite membranes. For example, when membranes are developed for reactors application, equilibrium between selectivity and permeance can be significant in terms of production and gas recovery (Lee *et al*. 2008). The range of properties between a Knudsen-like membrane and molecular sieving membrane can be considered for other types of applications to gas separation. For example, Shan and co-workers (Shan *et al*. 2007) reported the fabrication of meso- and macroporous membrane for bioprocessing applications. After a detailed fabrication method, a nanoporous membrane was obtained over a stainless steel disc and was slightly comparable with ultrafiltration membranes.

CMSMs have to be supported on ceramic or metallic supports to provide mechanical stability thus making them suitable for scaling-up. When a CMSM is pyrolyzed over porous supports, however, it is important to determine how the support influences the deposition of the polymer film and the resulting carbon layer. Depending on permeance it would be possible to manipulate the support during the fabrication process. However, few techniques allow for a non-destructive characterization of composite membranes during fabrication due to limitations in their detection ranges. LLDP has been successfully used for characterization of tubular composite membranes (Calvo *et al*. 2008) and it is a technique that allows for a non-destructive characterization of planar

or tubular supports. For this reason, we used this technique to observe the most important changes in the ceramic TiO_2 support when polymer or carbon layers are added. The technique is based on applying increasing pressures of a displacing fluid, which should be able to displace the wetting immiscible one from increasingly smaller pores. The relation between applied pressures, P, and radius of the pores successively being emptied, r, on each step pressure is given by the Cantor equation, which requires knowledge of the interfacial tension, γ, between wetting and displacing liquids.

$$P = \frac{2\gamma}{r} \tag{1}$$

Figure 6 presents the distribution of permeabilities versus pore size, which corresponds to the contribution (in percentage) of each pore size to the total permeability. It is possible to observe that for the uncoated support, the total flux is mainly governed by pore sizes in the range 2.5–4 nm. After the application of the polymer layer aged at 300 °C, the larger pores of the support are closed and a new population of pores in the range 2.1–2.5 nm governs the flow. After pyrolysis of the supported polymer membrane the flux decreases further, which indicates that it is governed by the pores with smallest sizes. These results agree with those reported by Sedigh *et al*. (2000) in the modification of an inorganic support with a carbon layer.

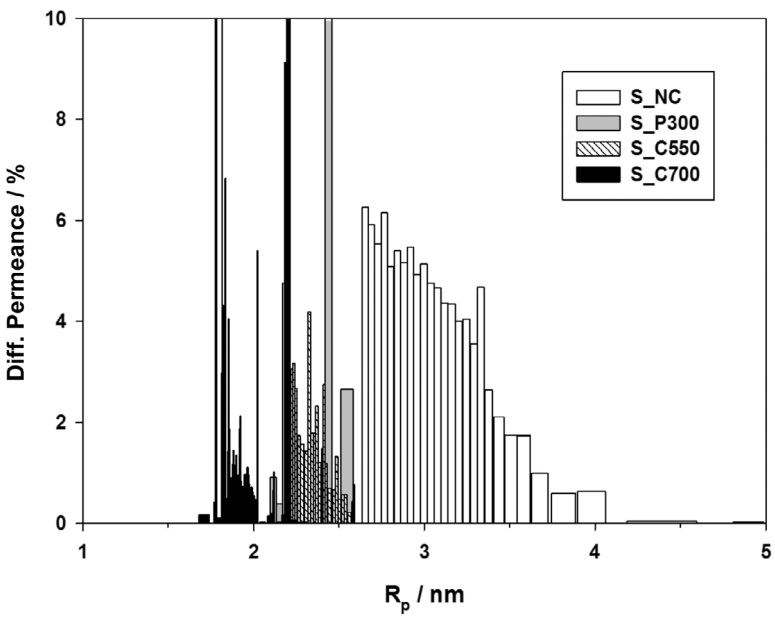

Figure 6. Permeability distribution for a Tami Support non-coated (S_NC), coated with polymer (S_P300), coated with carbon pyrolyzed at 550 °C (S_C550) and 700 °C (S_C700).

They reported a decrease in pore sizes of the support from 5.4 to 0.36 nm after carbon layer coating, as measured by N_2 adsorption. Figure 6 shows that the decrease of the largest micropores depends on the pyrolysis temperature, which in agreement with the results reported for unsupported carbon membranes (Lua and Su 2006). Samples pyrolyzed at 550 °C (2.3–2.6 nm)

seem to present bigger micropores than those pyrolyzed at 700 °C (1.7–2 nm). Even if this technique does not allow for the determination of ultramicropores, it is considered useful to determine the modification of the porosity of the support with polymer coating and carbon formation. Moreover, this type of characterization can be useful for optimization of fabrication methods to develop membrane for reactors application. Briceño *et al*. showed the suitability to apply this type of membranes for steam reforming of methanol in a membrane reactor configuration (Briceño *et al*. 2012b).

Figure 7 shows the molecular weight cut-off (MWCO) estimation of an original support and a composite membrane at different stages (polymer and carbon). The MWCO of the TiO_2 support was approximately 1600 Da, the difference with the nominal value reported by the manufacturer (1 kDa) attributable to the use of different measuring techniques. However, the relative differences between the uncoated ceramic support and the coated elements were quantified. Once a polymer layer is applied, MWCO decreased because the larger pores in the support were blocked by the polymer. A new porosity is thus created on the ceramic support depending on the pyrolysis temperature, as already explained in terms of the pore-size distributions. To summarize, the LLDP technique allows for detecting rearrangements in the structure of the support–coat ensemble due to the effect of pyrolysis temperature, and the consequent changes on porosity (Hayashi *et al*. 1995; Steel and Koros 2005).

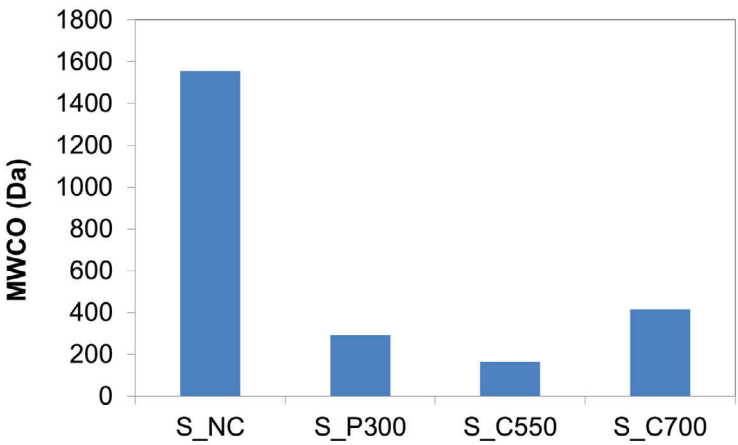

Figure 7. Molecular cut-off for TiO_2 support (S_NC), polymer-supported membrane (S_P300), carbon-supported membrane obtained at 550 °C and 700 °C (S_C550, S_C700).

Permeance and Selectivity of Carbon-supported Membranes

LLDP quantifies pores on the mesoporous and microporous ranges. However, to observe potential application on gas separation, it is necessary to plug big pores or possible defects that hinder effective CO_2 and CH_4 separation. Figure 8 shows permeance and selectivity values of two different types of supported carbon membranes with and without support interactions. In the case of supported carbon membranes obtained at 550 °C, permeances of CO_2 and CH_4 were $3.84 \times \cdot 10^{-8}$ and $6.15 \times \cdot 10^{-8}$ mol/m^2·Pa·s, respectively. This corresponds to an ideal selectivity factor of 0.62, slightly above the theoretical Knudsen selectivity value (0.60). High permeance and low selectivity suggest presence of defects in the composite membrane. In order to avoid repetitive and multiple carbon coating to obtain microporous membrane we wanted to observe the

separation capabilities of a single coating layer. For this reason, PDMS coating was applied onto the composite membranes.

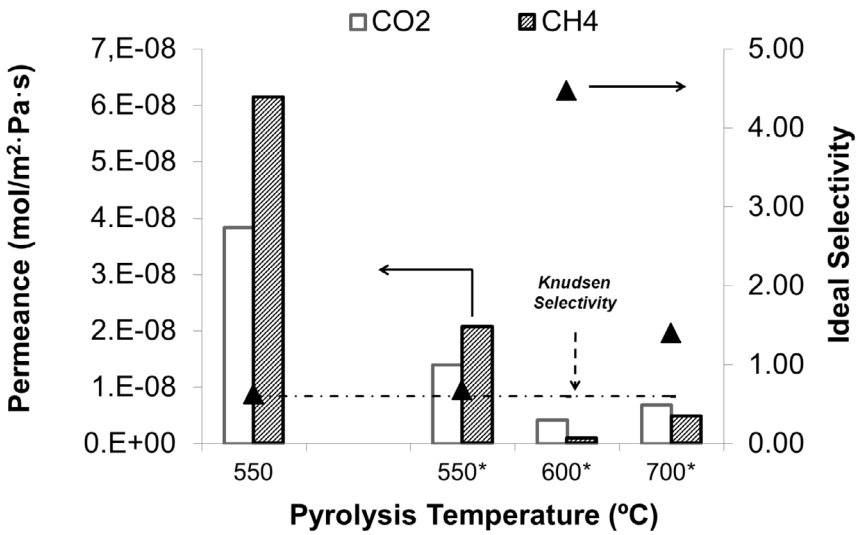

Figure 8. CO_2 and CH_4 permeance (bars) and ideal selectivity factors (closed triangles) for supported carbon samples obtained at 550°, 600° and 700 °C. * denotes samples with an additional PDMS coating. Values measured at 23 °C and 1 bar.

After pinholes or defect plugging with PDMS polymer, CO_2 and CH_4 permeance values decreased to 1.4×10^{-8} and 2.06×10^{-8} mol/m^2·Pa·s, respectively, with a small increase of the ideal selectivity factor to 0.68. The reason for this behaviour is that PDMS only plugs big defects leaving those pores with dimensions close to those of CO_2 and CH_4 molecules unaffected. However, at 550 °C microporosity formation is low, while increasing the temperature of pyrolysis increases microporosity. At 600 °C, PDMS plugging still produces low permeance values of 4.16×10^{-9} and 9.31×10^{-10} mol/m^2·Pa·s for CO_2 and CH_4, respectively, but a marked increase of the ideal selectivity factor to 4.47. Further increase of pyrolysis temperature would increase even more microporosity. However, at 700 °C both permeance and ideal selectivity factor decrease compared with those for the 650 °C sample. This was attributed to pore collapse, as established by the characterization of supported carbon samples by adsorption isotherms and calorimetry.

The PDMS coating allowed to evaluate the molecular sieving characteristics of the carbon layer supported on TiO_2/ZrO_2 tubes and it is clear that more research must be done in order to optimize the plugging method. This type of membrane could be used for high separation in gas purification or water treatment plants (Lee *et al*. 2008; Briceño *et al*. 2012a, b). The pore plug method offers a range of permeance and selective values that would be useful depending on the final membrane application.

CONCLUSIONS

Unsupported carbon membranes were produced at 550 and 700 °C. Adsorption–desorption show that pore size increases with pyrolysis temperature. By contrast, when the same polymer was

coated on porous ceramic supports, the pore and volume size decreased with pyrolysis temperature. Membranes on a porous support were prone to have an asymmetric structure that allowed for the formation of pores, which are different from that obtained for dense membranes. The effect of these differences in the fabrication of composite carbon-supported membranes was monitored by LLDP as a non-destructible and fast characterization technique allowing for a detailed characterization of the supports used. This information was completed with a not less detailed characterization of the pores of the carbon layer. In this case, immersion calorimetry allowed for differentiating between supported and unsupported samples. There was a heterogeneous nature of the samples evidenced by different pore-size distributions. The hysteresis found in both type of samples matched with the differences in heat of adsorption. Both temperature and the interactions with the support determined those differences.

The carbon structure obtained on porous ceramic support at 500 °C was still incipient, and contained pinholes and defects that caused small separation factors. After pore plugging, the effect of the defects was eliminated, and CO_2/CH_4 ideal separation selectivity rose above the theoretical values of a pure Knudsen-controlled transport.

ACKNOWLEDGEMENTS

The authors are indebted to the Spanish Government for financial support (Project CTQ2008-02491, partially funded by the FEDER program of the European Union) and to the commission of European Communities Specific OpenTok Project MTKD-LT-2005-030040. Special thanks to Mr. Enrique Gadea from the University of Alicante for his support on realization of experiments.

REFERENCES

Briceño, K., Garcia-Valls, R. and Montane, D. (2010) *Asia-Pac. J. Chem. Eng.* **5**, 169.
Briceño, K., Iulianelli, A., Montane, D., Garcia-Valls, R. and Basile, A. (2012b) *Int. J. Hydrogen Energy* **37**, 13536.
Briceño, K., Montane, D., García-Valls, R., Iulianelli, A. and Basile, A. (2012a) *J. Membr. Sci.* **415–416**, 288.
Calvo, J.I., Bottino, A., Capannelli, G. and Hernández, A. (2008) *J. Membr. Sci.* **310**, 531.
Calvo, J.I., Peinador, R.I., Prádanos, P., Palacio, L., Bottino, A., Capannelli, G. and Hernández, A. (2011) *Desalination* **268**, 174.
Centeno, T.A., Vilas, J.L. and Fuertes, A.B. (2004) *J. Membr. Sci.* **228**, 45.
Chagger, H.K., Ndaji, F.E., Sykes, M.L. and Thomas, M. (1995) *Carbon* **33**, 1405.
Favvas, E.P., Kouvelos, E.P., Romanos, G.E., Pilatos, G.I., Mitropoulos, A. Ch. and Kanellopoulos, N.K. (2007) *J. Porous Mater.***186**, 102.
Foley, H.C. (1995) *Microporous Mater.* **4**, 407.
Fuertes, A.B. (2000) *J. Membr. Sci.* **177**, 9.
Fuertes, A.B. and Centeno, T.A. (1999) *Carbon* **37**, 679.
Hayashi, J., Yamamoto, M., Kusakabe, K. and Morooka, S. (1995) *Ind. Eng. Chem. Res.* **34**, 4364.
Ismail, A.F. and David, L.I.B. (2001) *J. Membr. Sci.* **193**, 1.
Koresh, J.E. and Soffer, A. (1987) *Sep. Sci. Technol.* **22**, 973.
Lee, D.W., Park, S.J., Yu, C.Y., Ihm, S.K. and Lee, K.H. (2008) *J. Membr. Sci.* **316**, 63.
Lua, A.C. and Su, J. (2006) *Carbon* **44**, 2964.
Peinador, R.I., Calvo, J.I., Prádanos, P., Palacio, L. and Hernández, A. (2010) *J. Membr. Sci.* **348**, 238.
Rao, M.B. and Sircar, S. (1996) *J. Membr. Sci.* **110**, 109.

Rios, R.V.R.A., Silvestre-Albero, J., Sepúlveda-Escribano, A., Molina-Sabio, M. and Rodríguez-Reinoso, F. (2007) *J. Phys. Chem. C* **111**, 3803.
Rodríguez-Reinoso, F., Lopez-Gonzalez, J.D. and Berenguer, C. (1982) *Carbon* **20**, 513.
Saufi, S.M. and Ismail, A.F. (2004) *Carbon* **42**, 241.
Sedigh, M.G., Jahangiri, M., Liu, P.K.T., Sahimi, M. and Tsotsis, T.T. (2000) *AIChE J.* **46**, 2245.
Shan, T.N., Foley, H.C. and Zydney, A.L. (2007) *J. Membr. Sci.* **295**, 40.
Shimada, S., Yoshimatsu, M., Inagaki, M. and Otani, S. (1998) *Carbon* **36**, 1125.
Shirley, A.I. and Lemcoff, N. (1997) *AIChE J.* **43**, 419.
Silvestre-Albero, J., Gomez de Salazar, C., Sepulveda-Escribano, A. and Rodriguez-Reinoso, F. (2001) *Colloids Surf. A Physicochem. Eng. Asp.* **187–188**, 151.
Silvestre-Albero, A., Juárez-Galán, J.M., Silvestre-Albero, J. and Rodríguez-Reinoso, F. (2012) *J. Phys. Chem. C* **116**, 16652.
Sing, K.S.W., Everett, D.H., Haul, R.A.W., Moscou, L., Pierotti, R.A., Rouquerol, J. and Siemiewska, T. (1985) *Pure Appl. Chem.* **57**, 603.
Singh-Ghosal, A. and Koros, W.J. (2000) *J. Membr. Sci.* **174**, 177.
Steel, K.M. and Koros, W.J. (2003) *Carbon* **41**, 253.
Steel, K.M. and Koros, W.J. (2005) *Carbon* **43**, 1843.
Suda, H. and Haraya, K. (1997) *J. Phys. Chem. B* **101**, 3988.
Vu, De Q., Koros, W.J. and Miller, S.J. (2002) *Ind. Eng. Chem. Res.* **41**, 367.